Mice deficient in α-actinin-4 have severe glomerular disease

Claudine H. Kos,[1] Tu Cam Le,[1] Sumita Sinha,[2] Joel M. Henderson,[3] Sung Han Kim,[1] Hikaru Sugimoto,[4] Raghu Kalluri,[4] Robert E. Gerszten,[2] and Martin R. Pollak[1]

[1]Renal Division, Department of Medicine, Brigham and Women's Hospital and Harvard Medical School, Boston, Massachusetts, USA
[2]Cardiology Division and Center for Immunology and Inflammatory Diseases, Department of Medicine, Massachusetts General Hospital and Harvard Medical School, Boston, Massachusetts, USA
[3]Department of Pathology, Brigham and Women's Hospital and Harvard Medical School, Boston, Massachusetts, USA
[4]Program in Matrix Biology, Division of Gastroenterology, Beth Israel Deaconess Medical Center and Harvard Medical School, Boston, Massachusetts, USA

Dominantly inherited mutations in *ACTN4*, which encodes α-actinin-4, cause a form of human focal and segmental glomerulosclerosis (FSGS). By homologous recombination in ES cells, we developed a mouse model deficient in *Actn4*. Mice homozygous for the targeted allele have no detectable α-actinin-4 protein expression. The number of homozygous mice observed was lower than expected under mendelian inheritance. Surviving mice homozygous for the targeted allele show progressive proteinuria, glomerular disease, and typically death by several months of age. Light microscopic analysis shows extensive glomerular disease and proteinaceous casts. Electron microscopic examination shows focal areas of podocyte foot-process effacement in young mice, and diffuse effacement and globally disrupted podocyte morphology in older mice. Despite the widespread distribution of α-actinin-4, histologic examination of mice showed abnormalities only in the kidneys. In contrast to the dominantly inherited human form of *ACTN4*-associated FSGS, here we show that the absence of α-actinin-4 causes a recessive form of disease in mice. Cell motility, as measured by lymphocyte chemotaxis assays, was increased in the absence of α-actinin-4. We conclude that α-actinin-4 is required for normal glomerular function. We further conclude that the nonsarcomeric forms of α-actinin (α-actinin-1 and α-actinin-4) are not functionally redundant. In addition, these genetic studies demonstrate that the nonsarcomeric α-actinin-4 is involved in the regulation of cell movement.

J. Clin. Invest. **111**:1683–1690 (2003). doi:10.1172/JCI200317988.

Introduction

Focal and segmental glomerulosclerosis (FSGS) describes a pattern of renal injury observed as both a primary idiopathic entity and a secondary response to other primary disease processes (1). We previously demonstrated that in some families with autosomal dominant FSGS, disease is caused by mutations in *ACTN4*, which encodes α-actinin-4 (2). This disease is highly, but not fully, penetrant, leading to proteinuria and renal insufficiency in adulthood. Kidney failure develops in a significant fraction of family members heterozygous for *ACTN4* mutations. The mutant actinins show increased F-actin affinity (2). The glomerular visceral epithelial cells, or podocytes, appear to be the initial site of renal injury in these individuals. Two other recently described forms of human autosomal recessive kidney disease are also caused by defects in podocyte proteins. Neonates with defects in both nephrin alleles are born with severe nephrosis (3). Mutations in both podocin alleles are typically observed in children with an aggressive form of nephrosis and progressive kidney failure (4). Interestingly, mice homozygous for targeted disruption of CD2AP, a T cell adapter protein that interacts with both nephrin and podocin in the podocyte, have a similar phenotype (5). In the podocyte, CD2AP, nephrin, and podocin all localize to the slit diaphragm (5–8). Like CD2AP, α-actinin-4 is very widely expressed. However, for unclear reasons, the human phenotype associated with *ACTN4* mutations is apparent only in the kidney (2). Reasonable hypotheses include the possibility that a podocyte-specific protein-protein interaction is altered by human disease–associated mutations, or that the unique structure of podocytes makes this cell type more susceptible to a subtle change in cytoskeletal architecture.

There are four mammalian α-actinin genes, all of which encode highly homologous, approximately 100-kDa actin–cross-linking proteins that exist as head-to-tail dimers (9). Isoforms α-actinin-2 and -3 are expressed

Received for publication January 29, 2003, and accepted in revised form April 9, 2003.

Address correspondence to: Martin Pollak, HIM 534, 77 Avenue Louis Pasteur, Boston, Massachusetts 02115, USA.
Phone: (617) 525-5840; Fax: (617) 525-5841;
E-mail: mpollak@rics.bwh.harvard.edu.
Claudine H. Kos and Tu Cam Le contributed equally to this work.

Conflict of interest: The authors have declared that no conflict of interest exists.

Nonstandard abbreviations used: focal and segmental glomerulosclerosis (FSGS); blood urea nitrogen (BUN); glomerular basement membrane (GBM).

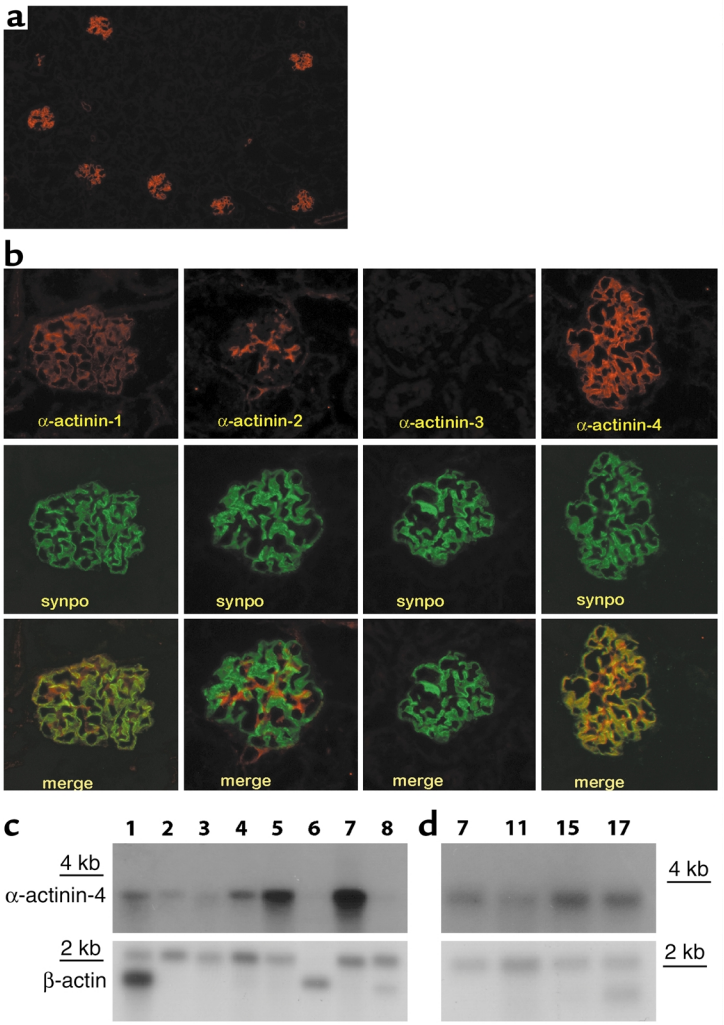

Figure 1
(**a**) α-Actinin-4 expression in mouse kidney shown at low power (image obtained at ×10 magnification). (**b**) Analysis of α-actinin-1, -2, -3, and -4 expression (red) and synaptopodin (synpo; green) in mouse kidney. Merged images are shown below. α-Actinin-1 and -4 show essentially podocyte-limited expression, whereas α-actinin-2 shows a different expression pattern, consistent with a mesangial cell localization. α-Actinin-3 is not expressed in the mouse glomerulus. α-Actinin-1, -2, and -4 are also expressed in the renal vasculature (not shown). Images were taken at ×40 magnification. (**c**) Northern blot showing expression of α-actinin-4 transcript in various mouse organs (using mouse multiple-tissue Northern blot from CLONTECH Laboratories Inc.). Lane 1, heart; 2, brain; 3, spleen; 4, lung; 5, liver; 6, skeletal muscle; 7, kidney; 8, testis. Hybridization to a β-actin control probe is shown below, with a single 2-kb band in most lanes and an expected 1.8-kb band present in heart, skeletal muscle, and testis. (**d**) Northern blot showing expression of α-actinin-4 at embryonic days 7, 11, 15, and 17. Hybridization to a β-actin control probe is shown below.

almost exclusively in the sarcomere. α-Actinin-1 and -4 are widely expressed, though only α-actinin-4 is significantly expressed in the human kidney (2). α-actinin-1 and -4 appear to have different subcellular localizations. The only clear difference in biochemical function between the four actinins is in the calcium sensitivity of the C-terminal EF hand (9). Honda et al. found that α-actinin-4 appears to be absent from focal adhesions and adherens junctions, where α-actinin-1 localizes (10).

In the process of developing a "knock-in" mouse with a familial FSGS–associated *Actn4* point mutation, we developed a mouse lacking detectable *Actn4* expression. These mice develop severely damaged podocytes and progressive glomerular disease. The cellular abnormalities are not limited to the kidney, as leukocytes from these mice demonstrate increased chemokinesis and chemotaxis. Our findings demonstrate that α-actinin-4 has a nonredundant role in cell movement and that α-actinin-4 is required for normal podocyte function. This α-actinin-4–deficient mouse provides a model both for the further study of α-actinin-4 and for studies of FSGS.

Methods

Mouse model development. We isolated a mouse genomic bacterial artificial chromosome (BAC) clone containing *Actn4* by screening an arrayed 129/SvJ genomic library by PCR. We subcloned an 11-kb *Hind*III genomic fragment containing *Actn4* exons 4–10 (Figure 2a). A loxP-flanked neomycin resistance cassette was inserted into an *Xho*I site 400 bp 3′ of exon 8 as shown. We mutagenized the sequence of exon 8 in order to both alter the encoded amino acid sequence (Lys256Glu) and add a silent *Ear*I restriction site to simplify genotyping (using a Stratagene QuickChange kit; Stratagene, La Jolla, California, USA). We electroporated 129/SvJ ES cells and selected for G418-resistant colonies. We screened 122 resistant colonies for an altered *Hind*III fragment by Southern blot using an external probe as shown in Figure 2a. We found four homologously recombinant colonies. We injected homologously recombinant cells from one colony into the C57BL/6 blastocysts of pseudopregnant mice (Brigham and Women's Hospital Transgenic Core facility), identified chimeric offspring, and bred these mice to C57BL/6 females. Initial

breeding to C57BL/6 mice produced several lines harboring the targeted allele, verified by Southern blot and/or PCR amplification and *Ear*I digestion. These offspring were on a mixed background, with a 50% contribution from 129/SvJ (the ES cell strain) and a 50% contribution from C57BL/6 (the strain to which the chimeras were bred).

Mouse genotyping. We isolated DNA from mouse tails. We genotyped mice by PCR amplification: mACTN4-Ex8(–122)-F: GGT TTC CAG TCC AAG AGA GGC CAC T; and mACTN4-Ex8(+64)-R: TGT GGG TCC TAA CAA GTG ATC TCA C; then mACTN4-Ex8(–93)-F: TCT GCA AGA GAA ATG AAG TGA GCG T; and mACTN4-Ex8(+64)-R: TGT GGG TCC TAA CAA GTG ATC TCA C; followed by digestion with *Ear*I (Figure 2b) and electrophoresis on an agarose gel.

Northern blot analyses. RNA was prepared from kidneys of newly sacrificed mice using Trizol reagent (GIBCO; Invitrogen Corp., Carlsbad, California, USA). Electrophoresis, transfer, and hybridization were performed using standard methods. A radiolabeled probe was generated from an RT-PCR amplicon corresponding to *Actn4* nucleotides 655–933 using primers F: GAT GAT CCA GTC ACC AAC CTA AAC and R: CCG AAT CCA CTC TAG AAG ATC AC (Figure 2c). Northern blot analyses were also performed using blots obtained from CLONTECH Laboratories Inc. (Palo Alto, California, USA) to examine *Actn4* RNA expression in various tissues and developmental stages (Figure 1, c and d).

Western blot analysis. We prepared protein from mouse kidney, lung, brain, liver, spleen, and cultured fibroblasts by homogenization in lysis buffer: 150 mM NaCl, 50 mM Tris (pH 8.0), 1% Triton X-100, Na orthovanadate, microcystin, and complete protease inhibitor (Roche Applied Science, Indianapolis, Indiana, USA). Western blot analyses were performed with antibodies to the N-terminal domains of α-actinin-1 and α-actinin-4 (described in ref. 2) using standard methods. Western blot of kidney lysates was also performed with a second α-actinin-4 antibody (raised against a peptide corresponding to amino acids 458–480) (11).

Histology. Freshly harvested kidneys were fixed in Bouin's solution. H&E staining was performed using standard methodology. Electron microscopy was performed after fixation in Karnovsky's media using standard diagnostic protocols. For the electron micrographs, all of the glomeruli that were imaged were from as deep into the renal cortex as possible. No incompletely differentiated glomerulus was imaged. We also performed necropsy of the remaining tissues by gross anatomic observation and light microscopy of tissues fixed in Bouin's solution. For analysis of mouse embryos, we sacrificed pregnant female mice for analysis of embryos at embryonic days 16.5–18.5 (counting the day of appearance of a vaginal plug as day 0.5).

Immunofluorescence. For these studies, fresh kidneys were embedded in Tissue-Tek OCT compound (Sakura Finetek, Torrance, California, USA), frozen in liquid nitrogen, and sectioned at 4 μm. Slides were fixed in cold 100% acetone or methanol and then air dried. Sections were then incubated with 1% BSA at room temperature to block nonspecific binding. They were next incubated with the primary antibodies at room temperature for 1 hour, rinsed with PBS, incubated with secondary antibodies at room temperature for 1 hour, and mounted with VECTASHIELD medium (Vector Laboratories Inc., Burlingame, California, USA). Staining was analyzed by fluorescence microscopy.

For the studies of actinin expression, we incubated anti–α-actinin-1, -2, -3, or -4 rabbit antisera (at 1:250 dilution) together with a mouse monoclonal anti-synaptopodin antibody (at 1:5 dilution; a gift of P. Mundel, Albert Einstein College of Medicine, New York, New York, USA) (12) with fixed sections of kidney from

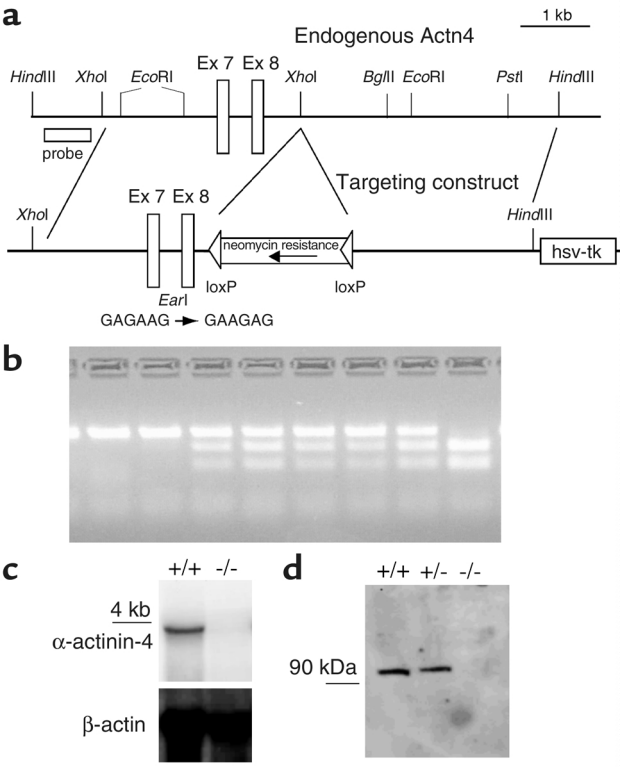

Figure 2
(**a**) Targeting construct. The construct used was originally designed for the development of a knock-in model. A neomycin resistance cassette is 438 bp from the 3′ end of exon (Ex) 8 of *Actn4*. (**b**) Genotyping assay. A PCR fragment amplified from wild-type genomic DNA does not digest with *Ear*I. The targeted allele has an *Ear*I site, allowing simple genotyping. The two left-hand lanes show this assay in two wild-type mice; the middle five lanes show amplification and digestion products of heterozygous mice. The final lane is derived from a mouse homozygous for the targeted allele. (**c**) Northern blot analysis of *Actn4* expression in mice homozygous for the wild-type allele (+/+) and for the targeted allele (–/–). Rehybridization of membrane with β-actin as a control for RNA loading is shown below. (**d**) Western blot of kidney lysates using anti–α-actinin-4 antibody. The same pattern was seen with lung, liver, brain, and spleen. No difference was seen in the expression of α-actinin-1 (not shown).

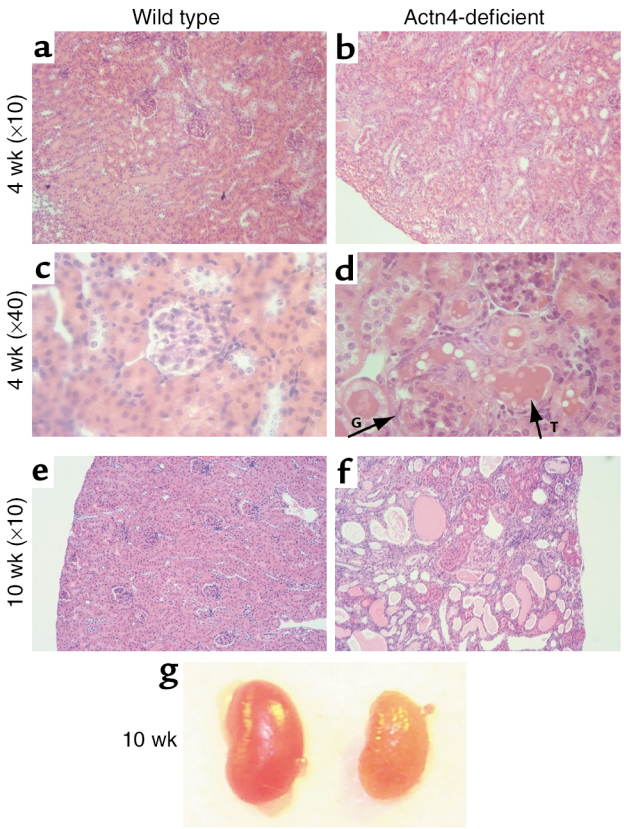

Figure 3
(**a** and **b**) Kidney sections from 4-week-old mice, stained with H&E. *Actn4*$^{+/+}$ kidney (**a**) and *Actn4*$^{-/-}$ kidney (**b**) photographed at ×10 magnification. (**c** and **d**) At higher magnification (×40), glomerular abnormalities are clearly visible in the *Actn4*$^{-/-}$ mouse (**d**), but not in the *Actn4*$^{+/+}$ littermate (**c**): the *Actn4*$^{-/-}$ kidney shows FSGS, with protein in tubules and areas of glomerular capillary collapse. A diseased glomerulus is indicated by an arrow (labeled "G"). A tubule filled with proteinaceous material is also indicated by an arrow (labeled "T"). (**e** and **f**) Kidney sections from 10-week-old mice, stained with H&E. (**e**) *Actn4*$^{+/+}$ kidney; (**f**) *Actn4*$^{-/-}$ kidney. The *Actn4*$^{-/-}$ kidney shows extensive disease, with sclerosed glomeruli, dilated tubules with proteinaceous material, and disrupted architecture. (**g**) Gross appearance of *Actn4*$^{+/+}$ (left) and *Actn4*$^{-/-}$ (right) kidneys from 10-week-old mice.

newly sacrificed wild-type mice. Isoform-specific anti-actinin antibodies were described previously (13). A secondary goat anti-rabbit Cy3-labeled antibody and a secondary hamster anti-mouse FITC-labeled antibody were used diluted 1:200 in PBS (Sigma-Aldrich, St. Louis, Missouri, USA) (Figure 1). We also performed immunofluorescence studies of kidneys from *Actn4*$^{-/-}$ mice after the onset of mild microalbuminuria (age 5.5 weeks) as well as kidneys from *Actn4*$^{+/+}$ sex-matched littermates. We used primary antibodies to nephrin and podocin, described in ref. 11. We used an anti–collagen type IV antibody obtained from ICN Biomedicals Inc. (Costa Mesa, California, USA). FITC-labeled secondary antibodies were purchased from Jackson ImmunoResearch Laboratories Inc. (West Grove, Pennsylvania, USA).

Biochemistry. Analyses of blood urea nitrogen (BUN) concentrations were performed in the Brigham and Women's Hospital Clinical Laboratory. Urine protein was assessed by dipstick (Albustix; Bayer Corp., Pittsburgh, Pennsylvania, USA) and/or by acrylamide gel electrophoresis and Coomassie blue staining.

Lymphocyte assays. We isolated lymphocytes from spleens of newly sacrificed mice and performed chemotaxis assays. The mice had no proteinuria or histologic evidence of kidney disease. Lymphocytes were placed in Transwell chemotaxis chambers (Neuro Probe Inc., Gaithersburg, Maryland, USA). Serial tenfold dilutions of chemokine mSDF-1 were added to the bottom wells. After 37°C incubation for 90 minutes, we counted cells migrating across the filter. Comparisons of migrating cells were analyzed by paired *t* tests using the results of four sets of independent experiments. We performed Western blot analysis of lymphocyte lysate using the anti–α-actinin-4 antibody.

Results

Expression of α-actinin-4. We performed immunofluorescence studies of α-actinin expression in mouse kidneys (Figure 1, a and b). In human kidney, we have observed significant expression of α-actinin-4 only (2). In mouse kidney, we observed strong expression of α-actinin-1 and α-actinin-4 in a podocyte pattern, colocalizing with the podocyte marker synaptopodin. In addition, α-actinin-2 was expressed in the glomerulus but in a different pattern, consistent with mesangial cell expression. Multiple-tissue Northern blot demonstrated α-actinin-4 expression in a variety of mouse tissues, with very strong expression in kidney and liver and strong expression in lung and heart (Figure 1c). Signal was minimal in skeletal muscle and testis and relatively low in brain and spleen. Northern blot analysis of mouse embryos demonstrated expression of α-actinin-4 as early as embryonic day 7 (Figure 1d).

We performed Northern and Western blot analysis to examine α-actinin-4 expression at the RNA and protein levels. By both Western blot and Northern blot analysis, we detected no expression of α-actinin-4 in the kidneys of mice homozygous for the targeted

Table 1
Genotype frequencies of mice, obtained in groups of litters of different age ranges

	E16.5–18.5	0–4 days	7–12 days	18–24 days
+/+	15 (12.25)	36 (31.25)	28 (23)	245 (189)
+/–	22 (24.50)	79 (62.5)	54 (46)	469 (378)
–/–	12 (12.25)	10 (31.25)	10 (23)	42 (189)
Total	49	125	92	756
–/– (% of total)	24.5%	8.0%	10.8%	5.6%

The relative frequencies of the different embryonic genotypes are not different from what is expected under mendelian inheritance (numbers in parentheses). The decrease in *Actn4*$^{-/-}$ mice after birth suggests perinatal lethality in a significant percentage of the *Actn4*$^{-/-}$ mice. E, embryonic day.

allele (Figure 2, c and d). Because we saw no detectable *Actn4* expression from the targeted allele, we refer to this allele as *Actn4*$^{-}$ for simplicity.

Phenotype. The genetic background of the original targeted mice (and littermates) derived from both the 129/SvJ ES cells and the C57BL/6 mice to which the chimeras were bred. Mice studied were on a mixed background, with approximately equal contributions from the 129/SvJ and C57BL/6 backgrounds.

We weaned and genotyped mice at approximately 3 weeks of age. Mice heterozygous for the targeted allele (*Actn4*$^{+/-}$) showed no obvious ill effect. We mated pairs of *Actn4*$^{+/-}$ mice. In contrast to the expected 25% frequency of homozygotes, we observed 1/18 of the offspring of *Actn4*$^{+/-}$ × *Actn4*$^{+/-}$ crosses to be homozygous for the targeted allele (42 of 756 pups; Table 1). We sacrificed newborn mice at 0–4 days of age. Ten of the 125 pups genotyped at days 0–4 were homozygous for the targeted allele (and, of these, 2 of 48 mice sacrificed at day 0–1 were homozygous). Approximately 10% of 7- to 12-day-old mice (10 of 92) were homozygous for the targeted allele. We also harvested embryos derived from similar heterozygous matings (embryonic days 16.5–18.5) and found 12 of 49 embryos to be homozygous for the targeted allele. We observed that in the initial weeks of life, those mice identified as *Actn4*$^{-/-}$ appeared grossly normal in appearance and behavior, but their rate of growth (compared with that of sex-matched littermates) frequently began to slow starting at approximately 6 weeks, and they subsequently began to lose weight.

Histology. Light microscopy (Figure 3) showed evidence of FSGS in kidneys of most *Actn4*$^{-/-}$ mice over 10 weeks of age. Kidneys of some mice showed areas of glomerular capillary collapse. Kidneys from these mice were typically small and pale on gross examination (Figure 3g). Transmission electron microscopy of *Actn4*$^{-/-}$ kidneys showed mild abnormalities at 5 weeks, including the development of areas of focal podocyte foot-process effacement and glomerular basement membrane (GBM) duplication (Figure 4). Slit diaphragms appeared normal. At later ages, the glomerular ultrastructure as visualized by transmission electron microscopy showed significant damage. We performed GBM thickness measurements in the *Actn4*$^{-/-}$ and control littermates and found no consistent differences between mice of different genotypes. We found no histologic abnormalities outside of the kidney in any of *Actn4*$^{-/-}$ animals sacrificed. Furthermore, we saw no renal or nonrenal abnormalities in any of the *Actn4*$^{-/-}$ mice sacrificed in late embryonic stages or in the sacrificed *Actn4*$^{-/-}$ neonatal mice.

We performed immunofluorescence using antibodies to podocin, nephrin, and type IV collagen and kidneys from *Actn4*$^{-/-}$ mice sacrificed shortly after the onset of microalbuminuria together with sex-matched *Actn4*$^{+/+}$ littermates. We found no consistent differences in expression of these proteins between *Actn4*$^{-/-}$ and *Actn4*$^{+/+}$ mice (Figure 5).

Biochemistry. As shown in Figure 6, we observed increasing albuminuria with advancing age in *Actn4*$^{-/-}$ mice but no significant albuminuria in *Actn4*$^{+/+}$ (or *Actn4*$^{+/-}$) littermates. The development of proteinuria was observed in most but not all mice by the time of sacrifice. Similarly, we observed increased BUN in many (but not all) of the *Actn4*$^{-/-}$ mice from blood obtained at the time of sacrifice (Figure 6).

Chemotaxis. α-Actinin-4 has been previously implicated in cell motility (10). Because leukocytes are easily isolated and can be studied directly without propagation in culture, we examined motility in these cells. As chemokines are potent dynamic modulators of the integrin-linked actin cytoskeleton, we assessed lymphocyte

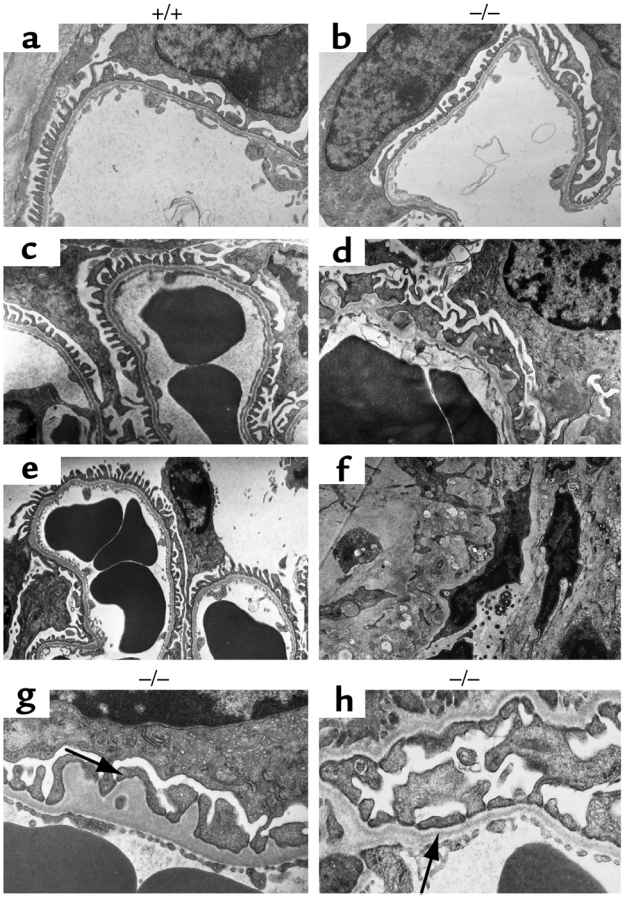

Figure 4
(**a** and **b**) Electron microscopic appearance of kidneys from 10-day-old *Actn4*$^{+/+}$ (**a**) and *Actn4*$^{-/-}$ (**b**) littermates. (**c** and **d**) Kidneys from 5-week-old *Actn4*$^{+/+}$ (**c**) and *Actn4*$^{-/-}$ (**d**) mice. (**e** and **f**) Kidneys from 10-week-old *Actn4*$^{+/+}$ (**e**) and *Actn4*$^{-/-}$ (**f**) mice. In all cases, *Actn4*$^{-/-}$ mice show altered glomerular ultrastructure. In the 10-day-old kidney (**b**), there is mild disruption of the normal podocyte structure with focal areas of podocyte effacement. The disease is more extensive in the older mice (**c** and **e**). (**g** and **h**) Early changes in *Actn4*$^{-/-}$ mice are shown at higher power. As shown in **g**, some *Actn4*$^{-/-}$ mice demonstrated areas with duplications, or "blebs," in the GBM on the subepithelial aspect (arrow). These abnormalities were not seen in the control mice, nor were they present in all *Actn4*$^{-/-}$ mice. In **h**, focal areas of foot-process effacement in an *Actn4*$^{-/-}$ mouse are evident (arrow).

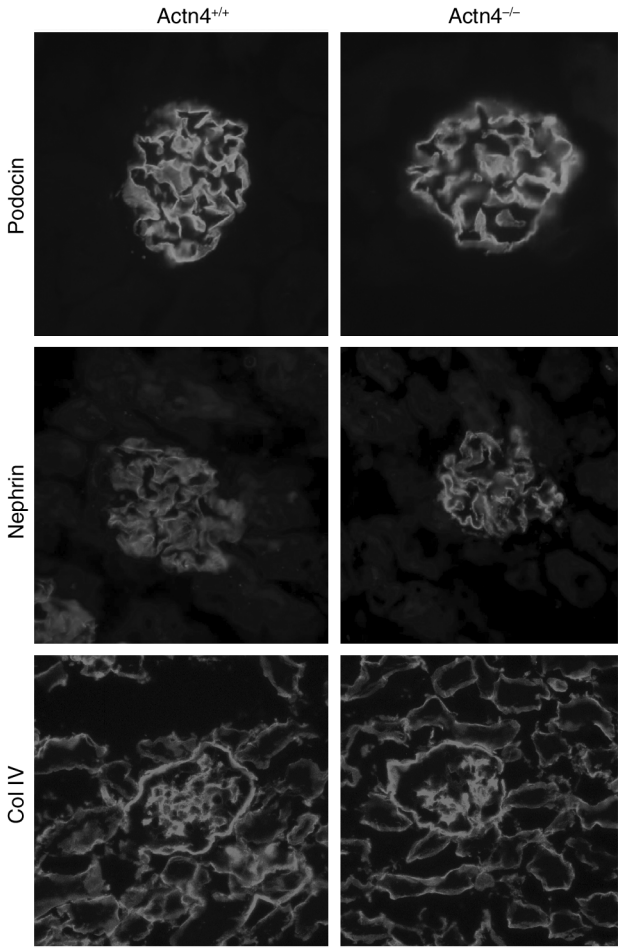

Figure 5
Immunofluorescence studies of kidneys from *Actn4*$^{-/-}$ mice and *Actn4*$^{+/+}$ littermates (×40 magnification). Antibodies to nephrin, podocin, and type IV collagen (col IV) have been previously described (11). Mice were 5.5 weeks of age at the time of sacrifice, and *Actn4*$^{-/-}$ mice had mild proteinuria.

motility by measurement of cell movement in response to chemokine SDF-1. We isolated murine lymphocytes from spleens of newly sacrificed mice and performed chemotaxis assays. As shown in Figure 7, we observed increased cell movement across filters in the *Actn4*$^{-/-}$ compared with the *Actn4*$^{+/+}$ cells in each of four independent sets of experiments. This difference was observed in unstimulated cells and was augmented by addition of chemokine (SDF-1). These findings were statistically significant (analyzed by two-tailed paired *t* test, $P < 0.005$). Flow cytometry demonstrated that there was an equal distribution of lymphocyte subsets from the mutant and control mice.

Discussion

In the process of developing a knock-in mouse model harboring a dominantly inherited α-actinin-4 mutation, we obtained a mouse model deficient in α-actinin-4. The development of this model was unintentional, though the disruption of normal gene expression by insertions of DNA into noncoding sequence is well described (14). The proportion of *Actn4*$^{-/-}$ mice observed from heterozygous matings was significantly less than expected under mendelian inheritance. The genotype ratios, however, were normal in late embryos. We conclude that a significant proportion of mice homozygous for the targeted allele do not survive the perinatal period. We do not know the cause of demise in these mice; histologic analysis of multiple *Actn4*$^{-/-}$ embryos and neonates showed no abnormalities. The mice that do survive the perinatal period go on to develop glomerular disease and progressive alteration in podocyte morphology, as well as proteinuria and eventual kidney failure. Heterozygotes for the targeted allele show no evidence of kidney disease at up to 6 months of age by the methods used for analysis of homozygotes.

As demonstrated, both α-actinin-1 and α-actinin-4 are expressed in the mouse podocyte. We had in fact anticipated that, because of their similar biochemistry and localization in mouse kidney, *Actn4* and *Actn1* would play redundant roles in mouse kidney. The results presented here demonstrate otherwise. We cannot discount the possibility that there remains a very low level of expression of *Actn4*$^{-/-}$ in these mice, below the level of our ability to detect expression, and that a standard *Actn4*$^{-/-}$ knockout would have an even more dramatic phenotype.

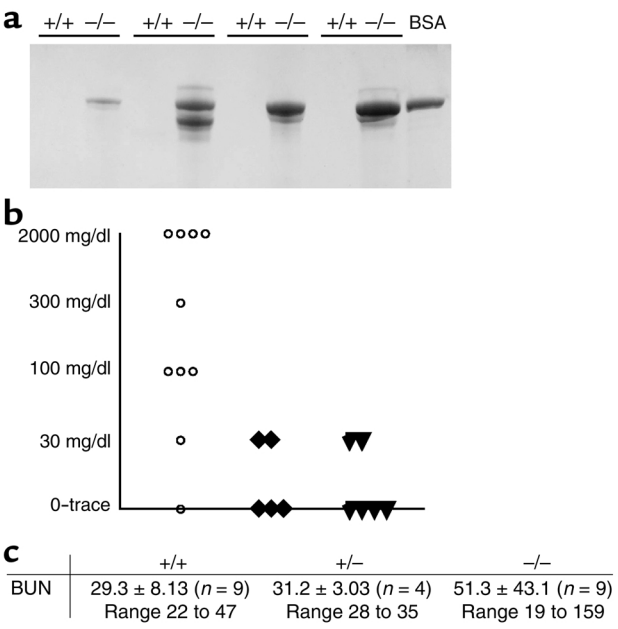

Figure 6
(**a**) Two microliters of mouse urine run on a 10% SDS-PAGE gel and stained with Coomassie. Urine from *Actn4*$^{-/-}$ mice is run next to urine from sex- and age-matched littermates. (**b**) Spot microalbumin measurements from mouse urine of different genotypes estimated by Albustix (Bayer Corp.). (**c**) Average BUN level, SD, and range, for *Actn4*$^{+/+}$, *Actn4*$^{+/-}$, and *Actn4*$^{-/-}$ mice.

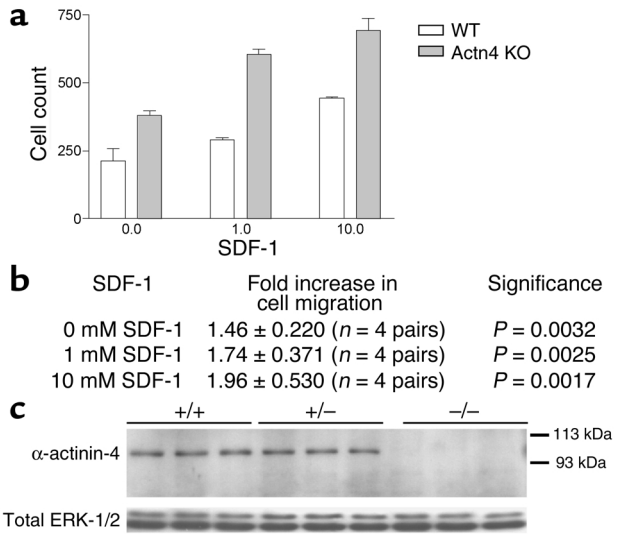

Figure 7

(**a**) Results of a representative chemotaxis assay. Lymphocytes were incubated with varying concentrations of SDF-1 as shown. Base-line movement is greater in the *Actn4*$^{-/-}$ cells, as well as in the *Actn4*$^{-/-}$ cells stimulated with 1 nmol and 10 nmol SDF-1. (**b**) Summary of all four sets of pairwise comparisons. Shown is the average increase in cell count in *Actn4*$^{-/-}$ expressed as a fraction of the cell count of *Actn4*$^{+/+}$ cells. (**c**) Western blot analysis of lymphocyte lysates from *Actn4*$^{+/+}$, *Actn4*$^{+/-}$, and *Actn4*$^{-/-}$ mice using an anti–α-actinin-4 antibody. Antibody to total ERK-1 and -2 served as a protein loading control.

Our previous human genetic studies suggested that gain-of-function mutations in α-actinin-4 can cause diseased podocytes and the development of FSGS. Humans with this form of disease are heterozygous for the mutant allele, which encodes a protein with greater-than-normal F-actin–binding activity (2). The results presented here indicate that alterations in α-actinin-4 can also cause mammalian disease by a loss-of-function mechanism. Like humans with *ACTN4*-associated disease, but unlike mice or humans with nephrin, podocin, or CD2AP defects (3–5, 11, 15), mice lacking *Actn4* do not have congenital nephrosis. This suggests that *Actn4* alterations lead to podocyte damage and FSGS by causing subtle cytoskeletal changes, rather than gross defects in the slit-diaphragm structure. This conclusion is supported by the lack of any dramatic changes in podocin and nephrin expression in these mice.

We initially attempted to perform motility assays in primary fibroblasts cultured from *Actn4*$^{+/+}$ and *Actn4*$^{-/-}$ mice. However, while we observed a trend toward increased motility in the *Actn4*$^{-/-}$ cells, there was great variability between assays, making us unable to draw any definitive conclusions. We therefore proceeded to perform chemotaxis assays in lymphocytes, because these cells are highly motile, are particularly sensitive to cytoskeletal changes, and can be assayed immediately after isolation, removing any potential artifacts that derive from propagation in cell culture. *Actn4*-deficient lymphocytes consistently displayed increased chemotaxis and chemokinesis. This suggests that α-actinin-4 plays a nonredundant role in cell motility. While we cannot make straightforward conclusions about the podocyte defect from altered lymphocyte behavior, this finding motivates further investigation into how the normal dynamics of the podocyte cytoskeleton depend on the presence of α-actinin-4. It is of interest that this is not the first molecule found to play critical roles in both lymphocytes and podocytes, as Shih et al. have previously shown a critical role for the T cell adapter protein CD2AP in podocyte function (5).

The altered motility observed in leukocytes and the altered podocyte structure may be different manifestations of the same biological perturbation. For example, motility is dependent on cell adhesion. Alterations in the adhesive properties of cells may lead to altered podocyte-GBM interactions, proteinuria, and more rapid lymphocyte movement. Furthermore, an altered podocyte-GBM interaction may alter the production of GBM matrix components, leading to the areas of abnormal GBM duplication ("blebs"; Figure 4) observed in some *Actn4*$^{-/-}$ mice. These hypotheses warrant further experimental investigation. Furthermore, the subtle alteration in chemotaxis observed in lymphocytes suggests the possibility that additional nonrenal phenotypes could be present that are not apparent by histologic analysis.

Absence of α-actinin-4 could also have a direct effect on the actin cytoskeleton. Decreased affinity of α-actinin for actin has been shown to alter the mechanical properties of actin–α-actinin gels (16). Absence of α-actinin-4 could have a similar effect, increasing the fluidity of the cytoskeleton and altering both cell motility (as we have observed in lymphocytes) and cell adhesion (leading to altered podocyte-GBM and podocyte-podocyte interactions).

Although we see a functional change in assays of lymphocyte function, the only clear physiologically and histologically significant phenotype we have observed in *Actn4*$^{-/-}$ mice that survived the neonatal period is the severe glomerular disease described. Despite careful histologic analysis of multiple *Actn4*$^{-/-}$ mice, we saw no other abnormalities. Why is this? Podocytes are unique cells, not unlike neurons, with large cell bodies, and axonlike projections that form functionally important processes (synapses in neurons, foot processes in podocytes) (17). The width of a podocyte foot process (about 120–150 nm) is much smaller than the width of most cells. The length of a rod formed by α-actinin dimers is approximately 40 nm. Thus there is a significant geometric constraint on α-actinin-4 in the podocyte. This constraint may cause the functions of α-actinin-4 in the podocyte to be different from its functions elsewhere.

Further studies will be required to understand the precise role of α-actinin-4 in glomerular function. However, the results presented here demonstrate that podocyte damage and proteinuria can result from

cytoskeletal alterations, rather than direct alterations in slit-diaphragm proteins. The fact that loss-of-function mutations, in addition to gain-of-function mutations, can lead to proteinuria and FSGS supports further investigation into the role that subtle inherited and acquired changes in α-actinin-4 may play in the development of human kidney disease.

Acknowledgments

This work was supported by grants from the NIH (DK-59588 to M.R. Pollak, HL-65584 to R. Gerszten, HL-07208 to S. Sinha, and DK-51711 and DK-55001 to R. Kalluri).

1. Ichikawa, I., and Fogo, A. 1996. Focal segmental glomerulsoclerosis. *Pediatr. Nephrol.* **10**:374–391.
2. Kaplan, J.M., et al. 2000. Mutations in ACTN4, encoding alpha-actinin-4, cause familial focal segmental glomerulosclerosis. *Nat. Genet.* **24**:251–256.
3. Kestila, M., et al. 1998. Positionally cloned gene for a novel glomerular protein — nephrin — is mutated in congenital nephrotic syndrome. *Mol. Cell.* **1**:575–582.
4. Boute, N., et al. 2000. NPHS2, encoding the glomerular protein podocin, is mutated in autosomal recessive steroid-resistant nephrotic syndrome. *Nat. Genet.* **24**:349–354.
5. Shih, N.Y., et al. 1999. Congenital nephrotic syndrome in mice lacking CD2-associated protein. *Science.* **286**:312–315.
6. Holzman, L.B., et al. 1999. Nephrin localizes to the slit pore of the glomerular epithelial cell. *Kidney Int.* **56**:1481–1491.
7. Ruotsalainen, V., et al. 1999. Nephrin is specifically located at the slit diaphragm of glomerular podocytes. *Proc. Natl. Acad. Sci. U. S. A.* **96**:7962–7967.
8. Schwarz, K., et al. 2001. Podocin, a raft-associated component of the glomerular slit diaphragm, interacts with CD2AP and nephrin. *J. Clin. Invest.* **108**:1621–1629. doi:10.1172/JCI200112849.
9. Takada, F., et al. 2001. Myozenin: an alpha-actinin- and gamma-filamin-binding protein of skeletal muscle Z lines. *Proc. Natl. Acad. Sci. U. S. A.* **98**:1595–1600.
10. Honda, K., et al. 1998. Actinin-4, a novel actin-bundling protein associated with cell motility and cancer invasion [erratum 1998, **143**:following 276]. *J. Cell Biol.* **140**:1383–1393.
11. Hamano, Y., et al. 2002. Determinants of vascular permeability in the kidney glomerulus. *J. Biol. Chem.* **277**:31154–31162.
12. Mundel, P., et al. 1997. Synaptopodin: an actin-associated protein in telencephalic dendrites and renal podocytes. *J. Cell Biol.* **139**:193–204.
13. Chan, Y., Tong, H.Q., Beggs, A.H., and Kunkel, L.M. 1998. Human skeletal muscle-specific alpha-actinin-2 and -3 isoforms form homodimers and heterodimers in vitro and in vivo. *Biochem. Biophys. Res. Commun.* **248**:134–139.
14. Feng, Y.Q., Lorincz, M.C., Fiering, S., Greally, J.M., and Bouhassira, E.E. 2001. Position effects are influenced by the orientation of a transgene with respect to flanking chromatin. *Mol. Cell. Biol.* **21**:298–309.
15. Putaala, H., Soininen, R., Kilpelainen, P., Wartiovaara, J., and Tryggvason, K. 2001. The murine nephrin gene is specifically expressed in kidney, brain and pancreas: inactivation of the gene leads to massive proteinuria and neonatal death. *Hum. Mol. Genet.* **10**:1–8.
16. Wachsstock, D.H., Schwartz, W.H., and Pollard, T.D. 1993. Affinity of alpha-actinin for actin determines the structure and mechanical properties of actin filament gels. *Biophys. J.* **65**:205–214.
17. Pavenstadt, H., Kriz, W., and Kretzler, M. 2003. Cell biology of the glomerular podocyte. *Physiol. Rev.* **83**:253–307.